The optical intersubband absorption bandgap in quantum wells embedded in an asymmetric microcavity

1999 J. Phys.: Condens. Matter 11 2471

(http://iopscience.iop.org/0953-8984/11/11/017)

J. Phys.: Condens. Matter **11** (1999) 2471–2480. Printed in the UK PII: S0953-8984(99)99817-X

The optical intersubband absorption bandgap in quantum wells embedded in an asymmetric microcavity

Xin Chen

Department of Physics, University of Manchester Institute of Science and Technology, PO Box 88, Manchester M60 1QD, UK

Received 1 December 1998

Abstract. On the basis of a non-local theory, the linear intersubband optical response in quantum wells embedded in an asymmetric microcavity is investigated. Starting from the Maxwell–Lorentz equations, the field in the quantum-well microcavity is derived, and the expression for the optical absorption is given. Detailed numerical simulations show that modifying the field modes via changing the number of distributed Bragg reflecting layers in front of the cavity can lead to significant change of the absorption spectrum: Rabi splitting of the absorption, more peaks appearing in the spectrum, even formation of an absorption bandgap, and the centre and width of the bandgap can be modified by changing the corresponding wavelength of the distributed Bragg reflecting layers.

1. Introduction

Due to the unique opportunity offered by the quantum-well microcavity structure, the optical properties of such a structure have attracted much attention for both fundamental physics and applications reasons [1–11]. In such a structure, the electrons and field are both confined in one direction by the quantum wells and the cavity, respectively. It thus allows us to carry out a study of the light–quantum-well interaction in such a manner that by detuning the coupling between the quantum wells and the modes of the optical field available in the microcavity, the interaction between the light and the quantum well can be well controlled. To date, most of the theoretical and experimental results have been concentrated on interband transitions [1–7]. Also, investigations of the non-linear response arising from interband transitions—second-harmonic generation and bistability—have been carried out [8–10]. For a detailed review, the reader is referred to reference [11].

Recently, the optical responses of quantum wells arising from intersubband transitions in quantum wells have also been explored [12–21]. It has been demonstrated that, to obtain an accurate prediction of optical properties of quantum-well structures, it is necessary to include the local-field effects—that is, the field in those structures has to be treated in a self-consistent manner [12]. Along such lines, the asymmetric shape of the photon drag current in quantum wells has been shown to be in good agreement with experimental results [15]; the influence of the radiative coupling among quantum wells on the linear absorption [16], second-harmonic generation [17], and photon drag [15] have also been studied; meanwhile the intrinsic optical bistability in single quantum wells due to local-field feedback has been investigated [18, 19]; the effects of magnetic and electric fields on the linear optical response have been explored as

0953-8984/99/112471+10$19.50

well [20, 21]. In this paper a local-field theory has been used to investigate the linear optical absorption of quantum wells embedded in an asymmetric microcavity.

This paper is organized as follows. In section 2, starting from the Maxwell–Lorentz equations, the expression for the field in each layer constituting the basic cavity is given, and the field in the quantum wells is determined via an integral equation. Then, by matching the boundary conditions, the field in the quantum-well microcavity structure is determined, and the determined field is used to calculate the quantum-well absorption. In section 3, on the basis of the theory developed in the previous section, detailed numerical calculations for different numbers of distributed Bragg reflecting layers in front of the microcavity are performed, and the influences of the narrowness of the microcavity on the intersubband absorption are shown.

2. Theoretical framework

Described in Cartesian coordinates, the basic structure under consideration is constructed of three layers (a/b/c) which are characterized by their dielectric constants:

$$\epsilon(z) = \begin{cases} \epsilon_{\mathrm{a}} & z < 0 \qquad \text{layer a} \\ \epsilon_{\mathrm{b}} & 0 < z < L \qquad \text{layer b} \\ \epsilon_{\mathrm{c}} & z > L \qquad \text{layer c} \end{cases} . \tag{1}$$

There are N quantum wells of well width d located in the central layer b, in which the first well is located at L_1; the widths of the barriers between adjacent wells are d_{b}, which is wide enough for the electronic coupling to be neglected. To enhance the discrimination of the microcavity, two stacks of distributed Bragg reflecting (DBR) layers are placed in front of and behind the basic cavity of length $L(\Delta)$; cf. figure 1.

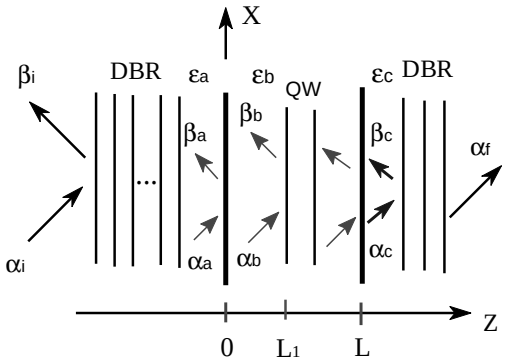

Figure 1. A schematic view of the quantum-well cavity structure.

In this paper, only a p-polarized (TM) incident field is applied to the structure, so the y-component of the field can be omitted in the following analysis. Let us first consider the field in the basic cavity structure, and deal with the effect of the DBR layers later. According to the Maxwell–Lorentz equations, the electric field in each layer is determined by the wave equations, and the electric field has the form

$$\vec{E}_\iota(z) = (\alpha_\iota \mathrm{e}^{\mathrm{i}q_\perp^{(\iota)} z} + \beta_\iota \mathrm{e}^{-\mathrm{i}q_\perp^{(\iota)} z})\vec{e}_x - \frac{q_\parallel}{q_\perp^{(\iota)}}(\alpha_\iota \mathrm{e}^{\mathrm{i}q_\perp^{(\iota)} z} - \beta_\iota \mathrm{e}^{-\mathrm{i}q_\perp^{(\iota)} z})\vec{e}_z \qquad \text{in layer } \iota = \text{a or c}. \tag{2}$$

Due to the presence of the quantum wells, the field in layer b is modified [13, 15–17]:

$$\vec{E}_B(z) = \vec{E}_{\mathrm{b}}(z) - \mathrm{i}\mu_0\omega \sum_{j=1}^{N} \int\int \overleftrightarrow{G}(z - z')\overleftrightarrow{\sigma}^{(j)}(z', z'')\vec{E}_B(z'')\,\mathrm{d}z''\,\mathrm{d}z' \tag{3}$$

where the background field, $\vec{E}_{\rm b}(z)$, is the field with no quantum wells in the central layer b, which has the same form as is given in equation (2).

$$\overleftrightarrow{G}(z-z') \qquad \text{and} \qquad \overleftrightarrow{\sigma}^{(j)}(z',z'')$$

are the appropriate propagator [12] and the non-local linear conductivity tensor of the wells. To specify the non-local conductivity tensor, it is assumed that in each quantum well there are two confined states in the conduction band, which is a good approximation when the incident photon energy is close to the energy separation considered. Of these two states, only the lower state is populated by electrons. Then it can be found from the density-matrix approach that the linear conductivity tensor takes a diagonal form, and the non-zero elements are given by [13]

$$\sigma_{xx}^{(j)}(z',z'') = \frac{\mathrm{i}e_0^2}{2\pi\overline{h}^2\omega}\frac{(\varepsilon_2^{(j)}-\varepsilon_1^{(j)})\left[E_F-\varepsilon_1^{(j)}\right]^2}{[\overline{h}(\omega+\mathrm{i}/\tau)]^2-\left[\varepsilon_2^{(j)}-\varepsilon_1^{(j)}\right]^2}\phi^{(j)}(z')\phi^{(j)}(z'') \tag{4}$$

$$\sigma_{zz}^{(j)}(z',z'') = \frac{\mathrm{i}e_0^2}{2\pi m\omega}\frac{(\varepsilon_2^{(j)}-\varepsilon_1^{(j)})(E_F-\varepsilon_1^{(j)})}{[\overline{h}(\omega+\mathrm{i}/\tau)]^2-\left[\varepsilon_2^{(j)}-\varepsilon_1^{(j)}\right]^2}\Phi^{(j)}(z')\Phi^{(j)}(z'') \tag{5}$$

and two abbreviations are introduced:

$$\phi^{(j)}(z) = \psi_1^{(j)}(z)\psi_2^{(j)}(z) \qquad \Phi^{(j)}(z) = \psi_1^{(j)}(z)\frac{\mathrm{d}\psi_2^{(j)}(z)}{\mathrm{d}z} - \psi_2^{(j)}(z)\frac{\mathrm{d}\psi_1^{(j)}(z)}{\mathrm{d}z}. \tag{6}$$

In the equations above, e_0 is the electron charge, m denotes the effective mass, τ is the relaxation time describing the intersubband transition dephasing process. $\varepsilon_2^{(j)}$ and $\varepsilon_1^{(j)}$ are the ground- and excited-state energies of the jth well, and $\psi_2^{(j)}(z)$ and $\psi_1^{(j)}(z)$ are the corresponding ground- and excited-state wavefunctions, respectively. On the basis of the global charge neutrality condition, the Fermi energy, E_F, can be obtained via

$$E_F = \varepsilon_1 + \frac{\pi\overline{h}^2}{m}N_s$$

where N_s is the surface electron density.

The tensor forms of the propagator and the conductivity allow us to rewrite equation (3) in matrix notation as

$$\vec{E}_B(z) = \vec{E}^{\rm b}(z) + \sum_{j=1}^{N}\overleftrightarrow{\Xi}^{(j)}(z)\vec{\gamma}^{(j)} \tag{7}$$

where

$$\overleftrightarrow{\Xi}^{(j)}(z) = \left[\int \overleftrightarrow{G}(z-z')\overleftrightarrow{T}^{(j)}(z')\,\mathrm{d}z'\right]\overleftrightarrow{\zeta}^{(j)} \tag{8}$$

$$\vec{\gamma}^{(j)} = \int \overleftrightarrow{T}^{(j)}(z'')\vec{E}_B(z'')\,\mathrm{d}z''. \tag{9}$$

The explicit expressions for $\overleftrightarrow{T}^{(j)}(z'')$ and $\overleftrightarrow{\zeta}^{(j)}$ are given by

$$\overleftrightarrow{T}^{(j)}(z) = \begin{pmatrix}\phi^{(j)}(z) & 0\\ 0 & \Phi^{(j)}(z)\end{pmatrix} \qquad \overleftrightarrow{\zeta}^{(j)} = \begin{pmatrix}\zeta_{xx}^{(j)} & 0\\ 0 & \zeta_{zz}^{(j)}\end{pmatrix} \tag{10}$$

and the non-zero elements of $\overleftrightarrow{\zeta}^{(j)}$ are given by

$$\zeta_{xx}^{(j)} = \frac{2m(E_F-\varepsilon_1^{(j)})}{\overline{h}^2}\zeta_{zz}^{(j)} = \frac{\mu_0 e_0^2}{\pi\overline{h}^2}\frac{(\varepsilon_2^{(j)}-\varepsilon_1^{(j)})\left[E_F-\varepsilon_1^{(j)}\right]^2}{[\overline{h}(\omega+\mathrm{i}/\tau)]^2-\left[\varepsilon_2^{(j)}-\varepsilon_1^{(j)}\right]^2}. \tag{11}$$

In the following, only the z-component of the field in layer b is considered. Noting that the x-component is slowly varying across the well [12] and assuming that the x-component is constant across the wells leads to $\gamma_x^{(i)} = 0$. Multiplying the z-part of the local field (equation (7)) with $\Phi^{(i)}(z)$ and thereafter integrating the resultant equation leads to

$$\overleftrightarrow{U}\gamma_z^{(i)} - \sum_{j=1}^{N} S_{zz}^{(i,j)}\gamma_z^{(j)} = -\frac{q_\parallel}{q_\perp^{(\mathrm{b})}}\left[\alpha_\mathrm{b}\int \Phi^{(i)}(z)\mathrm{e}^{\mathrm{i}q_\perp z}\,\mathrm{d}z - \beta_\mathrm{b}\int \Phi^{(i)}(z)\mathrm{e}^{-\mathrm{i}q_\perp z}\,\mathrm{d}z\right] \tag{12}$$

where

$$S_{zz}^{(i,j)} = \int \Phi^{(i)}(z)\,\Xi_{zz}^{(j)}(z)\,\mathrm{d}z.$$

Here it is assumed that the light is totally reflected at the interface b/c. Thus, $\alpha_\mathrm{c} = \alpha_f$, and $\beta_\mathrm{c} = 0$. In order to determine (as yet) unknown α_b and β_b, one has to match the boundary conditions—namely, the continuities of $E_x(z)$ and $D_z(z)$—at the interfaces: $z = 0$ and $z = L$. Thereafter, eliminating α_c and β_a in favour of α_b and β_b, and inserting α_b and β_b into equation (12), one finally obtains

$$\overleftrightarrow{U}\gamma_z^{(i)} + \sum_{j=1}^{N}\Gamma^{(i,j)}\gamma_z^{(j)} = \kappa^{(i)} \tag{13}$$

where

$$\Gamma^{(i,j)} = \left[\left(\int \Phi^{(i)}(z)\,\mathrm{d}z\,q_\parallel\right)\Big/\left[(1 + r_\mathrm{ab}r_\mathrm{bc}\mathrm{e}^{2\mathrm{i}q_\perp^{(\mathrm{b})}L})q_\perp^{(\mathrm{b})}\right]\right] \times \left[r_\mathrm{ab}(1 + r_\mathrm{bc}\mathrm{e}^{2\mathrm{i}q_\perp^{(\mathrm{b})}L})\,\Xi_{xz}^{(j)}(0) + t_\mathrm{ab}r_\mathrm{bc}\mathrm{e}^{\mathrm{i}q_\perp^{(\mathrm{b})}L}\,\Xi_{xz}^{(j)}(L)\right] - S_{zz}^{(i,j)} \tag{14}$$

and

$$\kappa^{(i)} = -\frac{\alpha_\mathrm{a}t_\mathrm{ab}q_\parallel(1 + r_\mathrm{bc}\mathrm{e}^{2\mathrm{i}q_\perp^{(\mathrm{b})}L})}{(1 + r_\mathrm{ab}r_\mathrm{bc}\mathrm{e}^{2\mathrm{i}q_\perp^{(\mathrm{b})}L})q_\perp^{(\mathrm{b})}}\int \Phi^{(i)}(z)\,\mathrm{d}z \tag{15}$$

where r_ab and r_bc are the amplitude reflection coefficients at interfaces a/b and b/c, respectively, and $t_\mathrm{ab} = 1 - r_\mathrm{ab}$.

With the knowledge of the local field in the quantum-well microcavity system, and according to the definition of the Fresnel reflection coefficient (R_p), the reflection reads

$$R_p = -\frac{\beta_\mathrm{a}}{\alpha_\mathrm{a}} = r_p - \frac{1 + r_\mathrm{ab}}{1 + r_\mathrm{ab}r_\mathrm{bc}\mathrm{e}^{2\mathrm{i}q_\perp^{(\mathrm{b})}L}}\sum_{j=1}^{N}\left[\Xi_{xz}^{(j)}(0) - r_\mathrm{bc}\mathrm{e}^{\mathrm{i}q_\perp^{(\mathrm{b})}L}\,\Xi_{xz}^{(j)}(L)\right]\gamma_z^{(j)} \tag{16}$$

where r_p is the reflection coefficient in the absence of the wells, which is given by

$$r_p = \frac{r_\mathrm{ab} + r_\mathrm{bc}\mathrm{e}^{2\mathrm{i}q_\perp^{(\mathrm{b})}L}}{1 + r_\mathrm{ab}r_\mathrm{bc}\mathrm{e}^{2\mathrm{i}q_\perp^{(\mathrm{b})}L}}.$$

In the absence of the quantum wells, the equations derived above, as expected, coincide with that for a standard three-layer structure. That is one of the reasons for which we deliberately consider the basic cavity first. The effects of DBR layers can be easily included via a transfer-matrix approach after obtaining the local field in the basic cavity. The amplitudes of the incoming field and the field immediately behind the DBR layer can be determined via the relation [22]

$$\begin{pmatrix}\alpha_i\\ \beta_i\end{pmatrix} = \overleftrightarrow{M}^n\begin{pmatrix}\alpha_\mathrm{a}\\ \beta_\mathrm{a}\end{pmatrix} = \overleftrightarrow{M}_n\begin{pmatrix}\alpha_\mathrm{a}\\ \beta_\mathrm{a}\end{pmatrix} \tag{17}$$

where $\overleftrightarrow{M}$ is the 2×2 transfer matrix, and n is the number of the paired layers constructing the DBR layer. It can easily be found that

$$r = -\frac{\beta_i}{\alpha_i} = \frac{M_n(2,2)R_p - M_n(2,1)}{M_n(1,1) - M_n(1,2)R_p}. \tag{18}$$

It can be seen from equation (18) that without a DBR layer in front of the cavity, namely when

$$\overleftrightarrow{M}_n = \mathbf{1}$$

we have $\alpha_i = \alpha_{\mathrm{a}}$ and $r = R_p$, as expected. Since the light is totally reflected at the interface b/c, the absorption A_p is thus determined via

$$A_p = 1 - |r|^2 = 1 - \left| \frac{M_n(2,2)R_p - M_n(2,1)}{M_n(1,1) - M_n(1,2)R_p} \right|^2. \tag{19}$$

3. Numerical results and discussion

In this section, detailed numerical calculations for the linear optical absorption arising from intersubband transitions are presented. The parameters used in the calculations are given as follows: the widths of the chosen $Al_{0.3}Ga_{0.7}As/GaAs$ quantum wells are $d = 80$ Å and $d_{\mathrm{b}} = 100$ Å, the electron density is 7×10^{11} cm^{-2}, and the normalizing factor is $\omega_{21} = (\varepsilon_2 - \varepsilon_1)/\hbar$. In the calculation of the eigenstates, the ratio 60:40 has been used for the split of the conduction and valence bands, and the potential bending due to the doping is neglected for simplicity. The quantum wells are located symmetrically in the cavity in all of the cases, and the width of the cavity is $L(\Delta) = \lambda_{21}$. The dielectric constants of layers a, b, and c are $\epsilon_{\mathrm{a}} = \epsilon_{\mathrm{b}} = 12.2$ ($Al_{0.3}Ga_{0.7}As$) and $\epsilon_{\mathrm{c}} = 1.0$ (vacuum). The materials constructing the front DBR layers are GaAs and $Al_{0.67}Ga_{0.63}As$; thus the dielectric constants are 13.1 and 11.0, respectively. The angle of incidence is 60°, and $\hbar/\tau = 3$ meV.

Figure 2 shows the intersubband absorption as a function of normalized photon energy for different numbers of DBR layers. The numbers of wells are: 1 (figure 2(a)), 20 (figure 2(b)) and 50 (figure 2(c)). The width of each of the DBR layers is chosen to be a quarter of $\lambda_\beta = \lambda_{21}$. The numbers of DBR layers are indicated in the figures. As shown in figure 2(a), with only one pair of DBR layers there is only one absorption peak in the spectrum, which is corresponding to the transition between the two confined states, and the spectrum shows a symmetric shape; the location of the peak is somewhat blue-shifted to $\sim 1.05\omega_{21}$ due to the local-field corrections [17]. Since in this case the cavity has a weak coupling with the quantum well, the system is in the so-called weak-coupling region—that is, the availability of continuum photon modes in the cavity is just slightly modified. With six pairs of DBR layers in front of the cavity, the Rabi splitting of the absorption occurs, and the size of the Rabi splitting is $\sim 0.1\omega_{21}$. This therefore indicates that on increasing the field confinement, the enhanced interaction between the quantum well and the cavity leads to a Rabi splitting, which is contrary to the conclusion [14] suggesting that only increase of the number of wells can yield Rabi splitting of intersubband transitions. It is also noticed that, due to the coupling of the quantum well and the microcavity, the location of the peak on the high-energy side is slightly blue-shifted in comparison with that of one-pair DBR layers. The amplitudes of the two peaks are roughly the same. With an increase of the number of DBR layers added to the cavity, the peak at $\sim 1.05\omega_{21}$ is then reduced and blue-shifted, and the Rabi-splitting peak at $\sim 0.95\omega_{21}$ is also blue-shifted and the amplitude is increased by more than a factor of two; two additional peaks appear in the spectrum. With more and more DBR layers added, this tendency becomes clearer; it is also noticed that the distances between the peaks are reduced; the valley between them centred at $\sim\omega_{21}$ is eventually developed into a bandgap.

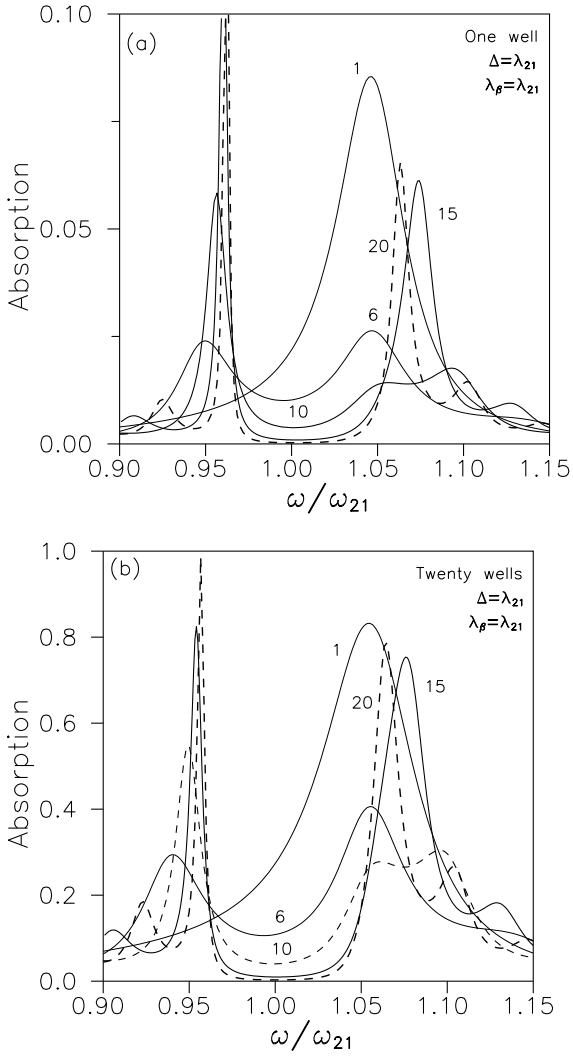

Figure 2. Absorption as a function of normalized photon energy for different numbers of DBR pairs. The numbers of wells are: 1 (a), 20 (b) and 50 (c). The width of each of the DBR layers is chosen to be a quarter of $\lambda_\beta = \lambda_{21}$. The numbers of paired DBR layers are shown in the panels.

In figure 2(b) there are twenty wells in the cavity, due to the radiative coupling among the quantum wells; the peak due to the transition between the bound states is blue-shifted and the HWHM (half-width at half-maximum) is greater than with that when there is only one well [16]. We note that if the local-field effects are neglected, the HWHM will remain constant, and this constant entirely depends on the value of $\overline{h}/\tau$ used (3 meV in this case). When six pairs of DBR layers are added to the cavity, the Rabi splitting is $\sim 0.102\omega_{21}$, larger than that when there is one quantum well, as was shown in the case of interband transitions [4]. An inspection of figure 2(b) shows that with the increase of the number of DBR layers, the peaks become narrower, and the distances between adjacent peaks become less, so more peaks appear in the fixed energy range; the HWHMs of the peaks on the lower-energy side are generally narrower than those of the peaks on the higher-energy side, while the absorption on the lower-energy

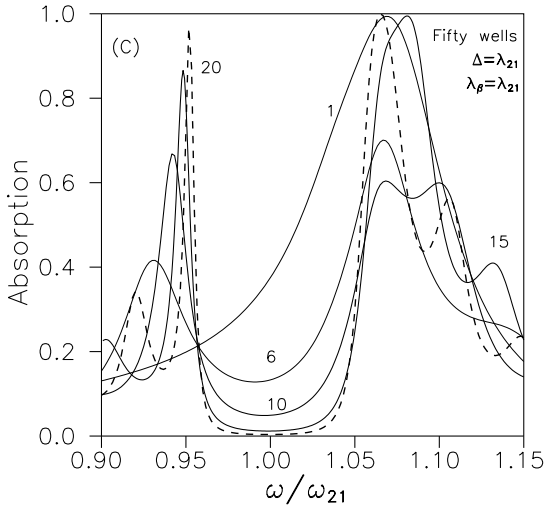

Figure 2. (Continued)

side is stronger than that on the higher-energy side; this asymmetric tendency becomes clearer as more DBR layers are added to the cavity due to the asymmetric nature of the microcavity.

With fifty quantum wells in the cavity, as shown in figure 2(c), in the case of one DBR layer in front of the cavity, the peak due to the intersubband transitions is located at $\sim 1.07\omega_{21}$ and the HWHM is considerably broadened as compared with those for the cases shown in figures 2(a) and 2(b). This can be understood by an inspection of equation (13): due to the strong radiative coupling among quantum wells [16, 17], the resonance conditions for $\gamma_z^{(i)}$ are different from well to well; that is, there is a distribution for $\gamma_z^{(i)}$, and the absorption peak shown in the spectra is due to the resonance of the $\gamma_z^{(i)}$, so the spectrum becomes broadened. Again, exclusion of the local-field effects leads to almost the same resonance condition for $\gamma_z^{(i)}$, since only the background field is slightly changed due to the change of the phase factor [16]. The Rabi splitting, which reaches $\sim 1.05\omega_{21}$, increases, as expected. From these figures it is found that the increase of the field confinement induced by means of adding more DBR layers in front of the cavity leads to there being fewer field modes available in the microcavity, indicating that fewer field modes can interact with the quantum wells in the cavity. Bearing in mind that the field is totally reflected at the interface b/c, in the case where no quantum well is embedded in the cavity there is no absorption; that is, the incoming light is totally reflected (no transmission). In all three situations, when the number of DBR paired layers becomes greater than fifteen, the absorption bandgap becomes apparent and the centre of the bandgap is at ω_{21}; this behaviour indicates that the field in the region close to ω_{21} is not available, although the quantum wells are able to absorb light in that region. It can also be seen that the field strength is greatly enhanced due to the strong cavity confinement, resulting in fewer field modes being available; this manifests itself via the strong peaks appearing on the lower-energy side.

Changing the corresponding wavelength of the front DBR paired layers to $\lambda_\beta = \lambda_{21}/1.05$—namely, at the absorption peak—leads to the centre of the absorption bandgap being at $1.05\omega_{21}$; this is shown in figure 3. The other parameters used are the same as for figure 2. With the change of the DBR layer widths, the field in the cavity is also correspondingly modified, and the peak due to the transition between the two bound states is blue-shifted. With six paired DBR layers put in front of the cavity, the Rabi splitting becomes smaller in comparison with that of figure 2(a), due to the splitting peak moving towards the peak due to the

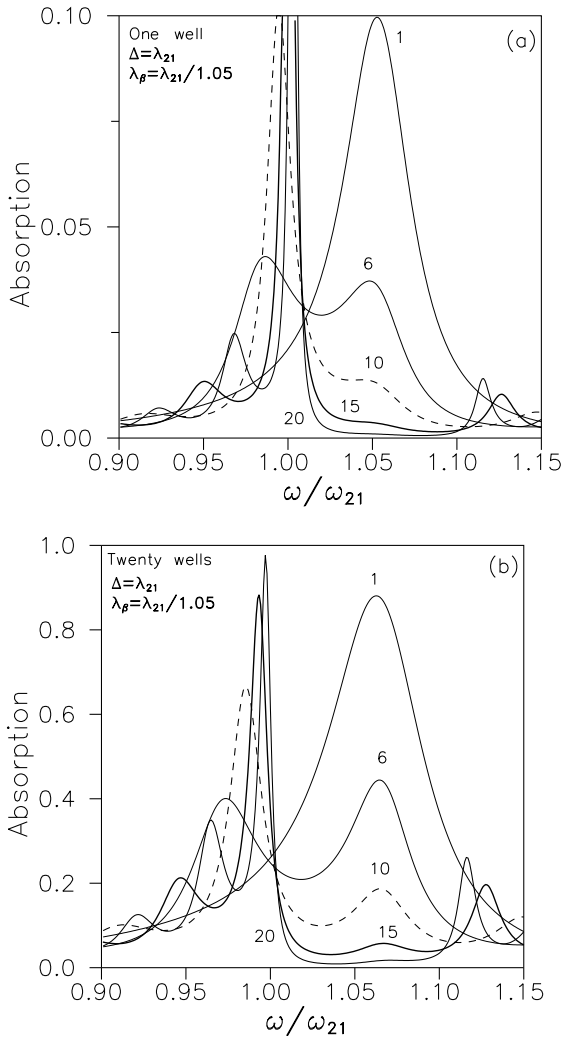

Figure 3. Absorption as a function of normalized photon energy for different numbers of DBR pairs. The numbers of wells are: 1 (a), 20 (b), and 50 (c). The width of each of the DBR layers is chosen to be a quarter of $\lambda_\beta = \lambda_{21}/1.05$. The numbers of paired DBR layers are shown in the panels.

transitions between the two bound states. Due to the enhancement of the field confinement, the peak at $\sim 1.05\omega_{21}$ is gradually smeared out, and the absorption bandgap is formed. As shown in figures 3(b) and 3(c), with more wells embedded in the cavity the absorption at $\sim 1.05\omega_{21}$ becomes stronger and the peak is blue-shifted; as a result, there is still a shoulder present at $\sim 1.08\omega_{21}$. As the field confinement is enhanced, it is found that more peaks appear in the spectrum and that the HWHM becomes broadened as the peaks move away from the bandgap.

In conclusion, the intersubband absorption in quantum wells embedded in an asymmetric cavity has been studied. By means of increasing the number of DBR layers in front the basic cavity, the field modes available to the quantum wells can be modified. Weak-, intermediate-, and strong-coupling (between the cavity and quantum wells) regimes are shown: it is found that for the weak-coupling regime there is only an symmetric absorption peak present in the

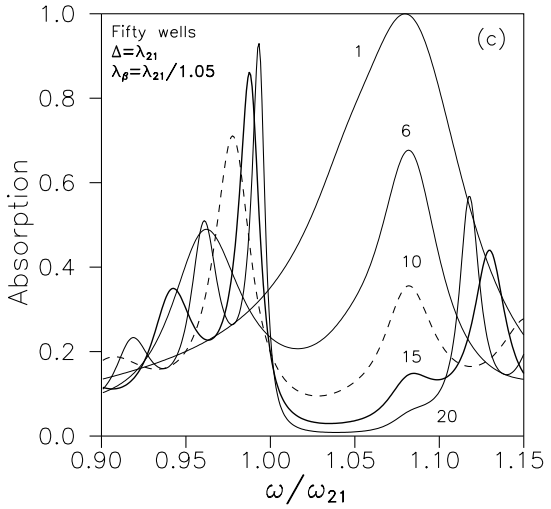

Figure 3. (Continued)

spectrum; in the intermediate-coupling regime the Rabi splitting occurs, even for the one-quantum-well case, and the Rabi splitting increases with the increase of the number of wells; for a high-finesse cavity the absorption bandgap is finally formed, and more absorption peaks appear in the spectrum, The width of the bandgap can be altered by changing the corresponding wavelength of the DBR layers.

References

[1] Weisbuch C, Nishioka M, Ishikawa A and Arakawa Y 1992 *Phys. Rev. Lett.* **69** 3314
[2] Citrin D S 1994 *IEEE J. Quantum Electron.* **30** 977 and references therein
[3] Panzarini G and Andreani L C 1995 *Phys. Rev.* B **52** 10 780
[4] Ivchenko E L, Kaliteevski M A, Kavokin A V and Nesvizhskii A I 1996 *J. Opt. Soc. Am.* B **13** 1061 and references therein
[5] Jorda S 1995 *Phys. Rev.* B **51** 10 857
Jorda S 1996 *Solid State Commun.* **97** 7
Jorda S 1996 *J. Opt. Soc. Am.* B **13** 1054
[6] Savona V, Andreani L C, Schwendimann P and Quattropani A 1995 *Solid State Commun.* **93** 733
[7] Fisher T A, Afshar A M, Whittaker D M and Skolnick M S 1996 *Microcavities and Photonic Bandgaps: Physics and Applications* ed J Rarity and C Weisbuch (Dordrecht: Kluwer) p 77
Fisher T A, Afshar A M, Whittaker D M and Skolnick M S 1995 *Phys. Rev.* B **51** 2600
Fisher T A, Afshar A M, Whittaker D M and Skolnick M S 1996 *Phys. Rev.* B **53** R10 469
[8] Tanaka T, Zhang Z, Nishioka M and Arakawa Y 1996 *Appl. Phys. Lett.* **69** 887
[9] Nakagawa S, Yamada N, Mikoshibo N and Mars D E 1995 *Appl. Phys. Lett.* **66** 2159
[10] Hubner B, Zengerle R and Forchel A 1995 *Appl. Phys. Lett.* **66** 3090
[11] Rarity J and Weisbuch C (ed) 1996 *Microcavities and Photonic Bandgaps: Physics and Applications* (Dordrecht: Kluwer)
Burstein E and Weisbuch C (ed) 1995 *Confined Electrons and Photons* (New York: Plenum)
Yokoyama H and Ujihara K (ed) 1995 *Spontaneous Emission and Laser Oscillation in Microcavities* (Boca Raton, FL: Chemical Rubber Company Press) and references therein
[12] Keller O 1996 *Phys. Rep.* **268** 85
Keller O 1997 *Prog. Opt.* **37** 257
[13] Keller O 1986 *Phys. Rev.* B **33** 990
[14] Liu A 1996 *Phys. Rev.* B **55** 7101
[15] Chen X and Keller O 1997 *Phys. Rev.* B **57** 15 706

Chen X 1998 *Phys. Scr.* **58** 377
[16] Chen X 1999 *IEEE J. Quantum Electron.* at press
[17] Chen X and Keller O 1997 *Phys. Status Solidi* b **203** 287
[18] Chen X and Xiao M F 1998 *Phys. Status Solidi* b **207** 551
[19] Chen X 1997 *Opt. Quantum Electron.* **29** 1023
[20] Chen X 1997 *J. Phys.: Condens. Matter* **9** 8249
Chen X 1998 *Phys. Scr.* **58** 107
[21] Chen X 1997 *Phys. Scr.* **57** 467
[22] Yeh P 1988 *Optical Waves in Layered Media* (New York: Wiley)